Journal of Materials Chemistry C

ROYAL SOCIETY OF CHEMISTRY

PAPER

View Article Online
View Journal | View Issue

Cite this: J. Mater. Chem. C, 2023, 11, 7772

A long-lived photoluminescent silver nanocluster-infused silver terephthalate metal organic framework with antibacterial and biofilm inhibition activity: a high functional resource†

Liz Hannah George,[a] Sreedharan Prathapan,[b] Narayanapillai Manoj,[b] Prasanth Rathinam,‡[c] Salbi Aadithya[d] and G. S. Sailaja *[ad]

Received 23rd March 2023,
Accepted 16th May 2023

DOI: 10.1039/d3tc01033c

rsc.li/materials-c

Functional materials with long-lived luminescence are extremely valuable due to their vast assortment of applications in optical devices, especially in bioimaging, sensors, security systems and other applications. A long-lived photoluminescent silver nanocluster-infused silver terephthalate metal organic framework (MOF) exhibiting green emission with a longer luminescent lifetime of 3.91 ms (ATP) was developed by a very facile and environmentally friendly method (room temperature, aqueous medium). The long-range array of silver nanoclusters deciphered from HRTEM and STEM images, both as embedded and as percolating out of the silver terephthalate MOF structure together with terephthalic acid ligand, primarily contributes to the longer lifetime of ATP. More interestingly, ATP is very photostable (for several months), which brings forward the scope of several customizable luminescent nanocomposite materials: films, hydrogels, thin film coatings, *etc.* Model systems were formulated to validate the luminescent property and customizability using base matrices poly(methyl methacrylate) (PMMA), polyvinyl alcohol and polycaprolactone. The intrinsic antibacterial and biofilm inhibition property of ATP befits it for antibacterial applications.

Introduction

Luminescent materials are of high demand owing to their versatility in advanced functional applications, while their glowing property opened several new puzzles in understanding the mechanism of the long-lived emission, which varies from system to system. Photoluminescence, the phenomenon involving the absorption of energy and subsequent emission of part of the absorbed energy in the form of light, is generally classified as fluorescence/phosphorescence based on the spin multiplicity of the excited state that is responsible for the light.[1] Fluorescence is a fast emission process with a nanoscale lifetime from singlet excited states, whereas phosphorescence is a slow process with higher lifetime attributed to the existence of comparatively stable triplet excited states.[2]

Long-lived luminescent materials, such as metals (rare earth/transition) oxides, carbon quantum dots, organic/inorganic phosphors, and others, are versatile candidates in emerging frontiers, *viz.*, bioimaging, chemical sensing, functional solids in light-emitting areas, phototherapy, data storage, security technologies, and others.[3–5] Ligands play a prime role in dictating the emission lifetime (from microseconds to minutes or even hours) when complexed with metals. For this reason, luminescence originates as a result of the ligand-centered emission/ligand-to-metal charge transfer/metal-to-ligand charge transfer/or guest-induced emission.[6] Ligand field emission is most commonly observed in highly conjugated organic systems, which enhances fluorescence emission by reducing the non-radiative transitions, while ligand-centered emission is commonly seen in transition metal-based metal organic frameworks.[7,8] Electron transfer from the ligand orbital to the metal orbital is termed as a ligand-to-metal charge transfer (LMCT).

Luminescent emissions of LMCT origin are sensitive to the structural characteristics and coordination geometry of materials. For example, terephthalic acid is a weakly fluorescent molecule. However, when coordinated to metal centers, it can

[a] Department of Polymer Science and Rubber Technology, CUSAT, Cochin 682022, India. E-mail: lizhannahgeorge@gmail.com
[b] Department of Applied Chemistry, CUSAT, Cochin, 682022, India. E-mail: prathapan@cusat.ac.in
[c] Pushpagiri Institute of Medical Sciences and Research Centre, Thiruvalla, 689101, India. E-mail: prasanthinam@gmail.com
[d] Inter University Centre for Nanomaterials and Devices, Cochin 682022, India. E-mail: sailajags@cusat.ac.in

† Electronic supplementary information (ESI) available. See DOI: https://doi.org/10.1039/d3tc01033c

‡ Health care and Life sciences business unit TATA ELXSI, Magarpatta, Pune.

affect luminescent properties by perturbations in the electronic states, as well as by modification of vibrational relaxations and other non-radiative processes. Alternatively, for metal complexes containing easily oxidized metals (Ag(I), Cu(I), *etc.*), the major cause for emission is metal-to-ligand charge transfer (MLCT).[7–9] The MLCT mechanism in such complexes is affected by the nature of functional groups attached to the organic ligands.

The emission lifetimes of common luminescent materials are in the range of nanoseconds to 10 μs. Neutral Pd(II) and Au(II) complexes exhibiting long lived green phosphorescence with an emission lifetime span of 100 μs have found applications in photocatalytic C–H functionalization, energy conversion and organic light-emitting diodes (OLEDs).[10,11] Lanthanide (III) ions have gathered considerable interest in bioimaging applications owing to their long emission lifetimes. The excellent luminescent behavior of lanthanide ions arises from 4f–4f electronic transitions. Eu^{3+} is the most commonly used Ln^{3+} since it shows millisecond range luminescence in the bright red region of the electromagnetic spectrum.[12]

Since ancient times, silver and its compounds have been considered attractive and widely accepted on account of their unique features, including their antibacterial, antifungal, and antiviral properties.[13,14] Molecular orbital studies carried out by Wang and co-workers on luminescent Silver(I) chalcogenide clusters proposed a ligand-to-metal charge transfer as the origin of luminescent emission.[15] Meanwhile, Jia *et al.* reported that the average lifetime of a thiolated silver nanocluster is on the microsecond scale, and the reason is attributed to the ligand-to-metal charge transfer (LMCT) or metal-to-ligand charge transfer (MLCT), followed by radiative relaxation through triplet excited states.[16] A similar study was conducted by Chen *et al.* on the photoemission mechanism of silver carboxylate nano clusters, and supports the LMCT mechanism. In other words, electron transfer from the oxygen atom in the carboxylate ligands to the Ag(I) ions to the silver atoms is followed by radiative relaxation, *i.e.*, ligand-to-metal (Ag^+)-to-metal (Ag atom) charge transfer takes place.[17]

Luo *et al.* constructed a one-dimensional zipper-like structured sky-blue luminescent silver(I) complex. The distance between the two silver atoms bridged by 2-diphenylphosphinopyridine (dppy) and thiocyanate ligands was found to be less than that of the van der Waals radii of two silver atoms, which suggests that the presence of strong argentophilic interactions in turn significantly contributes towards the luminescence exhibited by the compound. This mechanism could be extended to similar silver(I) complexes as well.[18]

In 2018, Grandjean *et al.* investigated the photoluminescence of a few atom silver clusters confined in LTA zeolites.[19] The bright green luminescence is dependent on several factors, such as interactions with the ligand oxygen, electrostatic interactions, electron confinement and electron transfer between the metal and ligands. The decay time indicates the existence of long-lived triplet states characteristic for spin forbidden transitions.[19] By varying the experimental conditions, silver nanoclusters with multicolour emissions have presented fascinating research to the world and paved the way for advanced functional materials of silver with luminescent effects along with its unique properties. Silver-based luminescent materials can be therefore proposed as potential alternatives for conventional luminescent materials.

Here, we introduce a long-lived silver based luminescent MOF with an unprecedented emission lifetime of millisecond range. Merging the unique properties of silver, the long-lived luminescent MOF could serve as a resource for the development of advanced functional materials.

Experimental section

Materials

Silver nitrate ($AgNO_3$) was purchased from Spectrochem. Terephthalic acid and PCL (M_w = 80 000) were purchased from Sigma Aldrich, and triethylamine was obtained from Merck. Polyvinyl alcohol was procured from SD Fine Chem. Ltd. PMMA with molecular weight M_n 6302 and M_w 12 107 Da was used for the preparation of films.

Methods

Synthesis of silver terephthalate MOF (ATP). ATP was synthesized by an environmentally-friendly aqueous one-pot method at room temperature. $AgNO_3$ (18 mmol) and terephthalic acid (36 mmol) in N_2 purged milli Q water (900 mL) were allowed to react at room temperature. After stirring for 5 min, 2 mL triethylamine was introduced dropwise to the reaction mixture and continued stirring for another 1 h. The obtained off-white product was washed with DMSO and subsequently with water until all residual reagents were washed away, and dried at 50 °C and labeled as ATP.

Preparation of the ATP–PMMA nanocomposite films. PMMA with a molecular weight of M_n 6302 and M_w 12 107 Da was used for the fabrication of nanocomposite films and coatings. Films with varying ATP concentrations (ATP–PM 12/5, ATP–PM 12/10 and ATP–PM 12/15) were prepared by dispersing 5, 10, and 15 wt% of ATP respectively in 12 wt% of PMMA solution in toluene. All solutions were sonicated and film casting was done in glass moulds and dried. PMMA/ATP thin films were prepared by drop casting 6 wt% PMMA solution in toluene containing 15 wt% of ATP. The obtained thin films were observed in a UV chamber.

Preparation of ATP–PCL thin film coatings. Briefly, ATP (0.045 g) was dispersed in 6 wt% of PCL (M_w = 80 000) solution in toluene. ATP–PCL (500 μL) solution was drop casted on clean glass slides and allowed to dry at room temperature. The hydrophilicity of the film was compared with that of the control PCL film by contact angle measurements.

Preparation of the ATP–PVA hydrogel. For the preparation of the hydrogel, 10 wt% PVA solution was prepared by adding PVA (2 g) in water (20 mL). ATP (12 wt%) was added to this solution, stirred and sonicated until a uniform dispersion was obtained. ATP–PVA films were prepared using a glass mould and dried at 60 °C. The films were cut into small pieces and dipped in

glyoxal (4 wt%) solution until it softened, and became elastic in nature. Films were then stacked in a cylindrical mould to fuse together, and were dried at 37 °C for 2 h. Luminescence of the hydrogels formed was observed upon UV irradiation.

Determination of the minimum inhibitory concentration (MIC) and sub-MIC selection. MIC assessment of ATP was done against the reference strain *P. aeruginosa* PAO1 (ATCC 10145) and two clinical isolates of *P. aeruginosa* RRLP1 (GenBank ID: KR149278) and *P. aeruginosa* RRLP2, (GenBank ID: KT309033). Determination of MIC was performed following the microdilution method, as recommended by the Clinical and Laboratory Standards Institute (CLSI 2006). Sterile media and media with ATP served as controls. In brief, an overnight bacterial culture of *P. aeruginosa* PAO1 (OD600 = 0.1) was diluted in Muller Hinton (MH) broth to prepare a standard inoculum of 1.5×10^8 CFU mL^{-1}. ATP was also diluted to attain a concentration ranging from 1.1275 mg mL^{-1}–0.0398 mg mL^{-1}, and incubated with the prepared standard inoculum for 24 h at 37 °C under shaking (100 rpm) condition. Following 24 h incubation, the optical density (OD) was measured at 600 nm to determine the MIC levels. For the biofilm inhibition studies, sub-MIC doses of ATP were used.

Biofilm inhibition study using the crystal violet staining method. A biofilm inhibition assay was performed as described earlier.[20] Biofilms by *P. aeruginosa* PAO1, RRLP1 and RRLP2 and A78 and A80 (*Acinetobacter baumannii* strains) were allowed to develop in a 96-well standard microtiter plate (MTP) having flat bottom wells without (control) and with (test) 0.16 mg mL^{-1} and 0.0797 mg mL^{-1} levels of ATP. Approximately 1×10^6 CFU mL^{-1} test bacterial cultures were inoculated into the LB broth and incubated for 24 h at 37 °C. After incubation, the planktonic cells were removed, and the wells were washed three times with distilled water and air dried. The adhered biofilms in the MTP wells were stained with 0.4% (w/v) crystal violet (CV) solution. Excess CV from the wells was removed using distilled water. Furthermore, CV from the adhered cells was solubilized using 95% (v/v) ethanol. Absorbance was measured at the wavelength of 570 nm and the percentage biofilm inhibition was calculated using eqn (1):

$$\% \text{ inhibition} = \frac{(\text{Control OD570} - \text{Test OD570})}{\text{Control OD570}} \times 100 \quad (1)$$

Physico-chemical characterizations. X-ray diffraction patterns of the samples were obtained using a Bruker D8 Advance Twin–Twin instrument with a step size of 0.020° and with Cu Kα radiation of wavelength 1.54 Å. Fourier transform infrared spectra were recorded on a PerkinElmer spectrum 20 FT-IR spectrophotometer in the frequency range of 400–4000 cm^{-1}. Attenuated total reflectance spectra were acquired using a Thermo Nicolet iS50 instrument using a diamond crystal. High-resolution transmission electron microscopic (HR-TEM) images were taken using a JEOL/JEM 2100 instrument. Scanning transmission electron microscope-high-angle annular dark-field (STEM-HAADF) images were obtained using a JEOL JEM-F200 transmission electron microscope. Thermal stability of the samples was analysed using a thermogravimetric analyzer TA Q50 by heating the samples to 800 °C with a heating rate of 20 °C min^{-1} under N_2 atmosphere. X-ray photoelectron spectroscopy (XPS) PHI 5000 Versa Probe II (ULVAC-PHIInc.) installed with a micro-focused (100–200 μm, 15 kV) monochromatic Al Kα X-ray source ($h\nu$ = 1486.6 eV) was used to determine the elemental composition of the samples. Photoluminescence spectra were taken on a Horiba Fluorolog 3 Spectrofluorometer with excitation and emission slit widths of 3 nm and 1.5 nm respectively. Phosphorescence spectra were taken using a laser attached to a spectrofluorometer with time-correlated single photon counting (TCSPC). The phosphorescence lifetime was recorded using the above spectrofluorometer equipped with a pulsed laser diode. Contact angle measurements were carried out using goniometry (Rame-Hart 187 Instrument Co.).

Results and discussion

The long lived silver nanocluster-infused silver terephthalate metal organic framework (ATP) was synthesized by a simple one-pot synthesis using silver nitrate and terephthalic acid. The ultrastructural characteristics and organization of the unit building blocks of ATP are manifested from TEM (Fig. 1a–d) and STEM (Fig. 2a and e) images. In the low magnification TEM image (Fig. 1b), besides the long-range array of ATP, a few larger silver nanoparticles are also visible that might be due to the reduction of Ag^+ ions in the presence of triethylamine. Meanwhile, the regular distribution of silver atomic clusters both as embedded on and percolating out of the MOF skeleton is clearly deciphered from the STEM elemental mapping images (Fig. 2a–h). The Ag nanoclusters are found to be nucleated and anchored on the host surface of MOF during

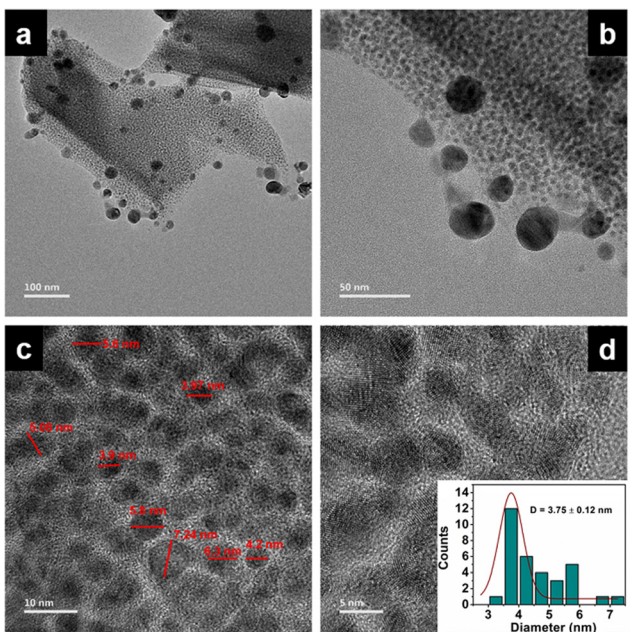

Fig. 1 (a–d) TEM images of ATP at different magnifications.

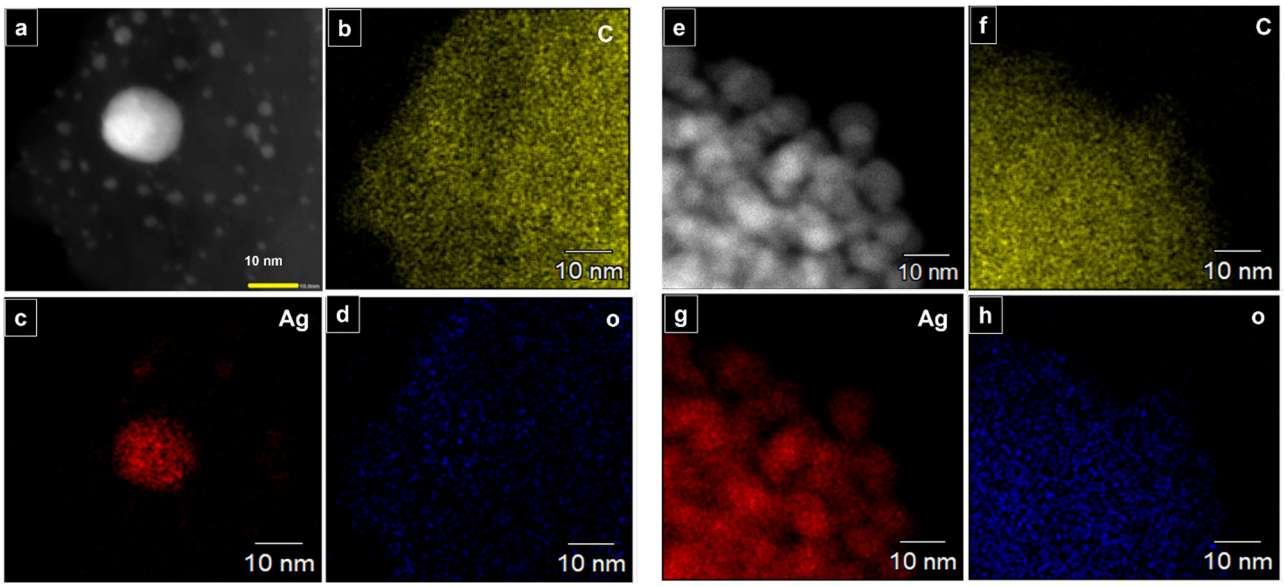

Fig. 2 (a–h) STEM elemental mapping of ATP: C, Ag, and O atoms indicating presence of infused silver nanoclusters in ATP.

the synthesis. The individual silver nanoclusters are of spherical shape with an average size of 3.75 ± 0.12 nm, which appeared to be well distributed. This was corroborated by the elemental mapping of high angle annular dark field STEM images of ATP (Fig. 3). It is hypothesized that the existence of these stable Ag nanoclusters contributes to the enhanced photoluminescence of ATP. The basic crystalline structure of ATP confirmed from powder XRD spectrum (Fig. 4a) matches well with that of $[Ag(BDC)_{1/2}]$, a silver coordination polymer.[21] Peaks at 13.09°, 16.4°, 18.02°, 18.7°, 25.0°, 25.5°, 27.1°, 28.3°, 30.9°, 32.2°, 33.7°, 34.1°, 40.4° and 42.6° correspond to the (100), (110), (011), (111), (021), (111), (211), (210), (121), (012), (031), (131), (100), (302) and (213) planes, respectively. The building block of ATP comprises carboxylate ions of two terephthalate molecules, which are bonded to two bridged silver ions. Each silver ion of ATP is linked to three oxygen

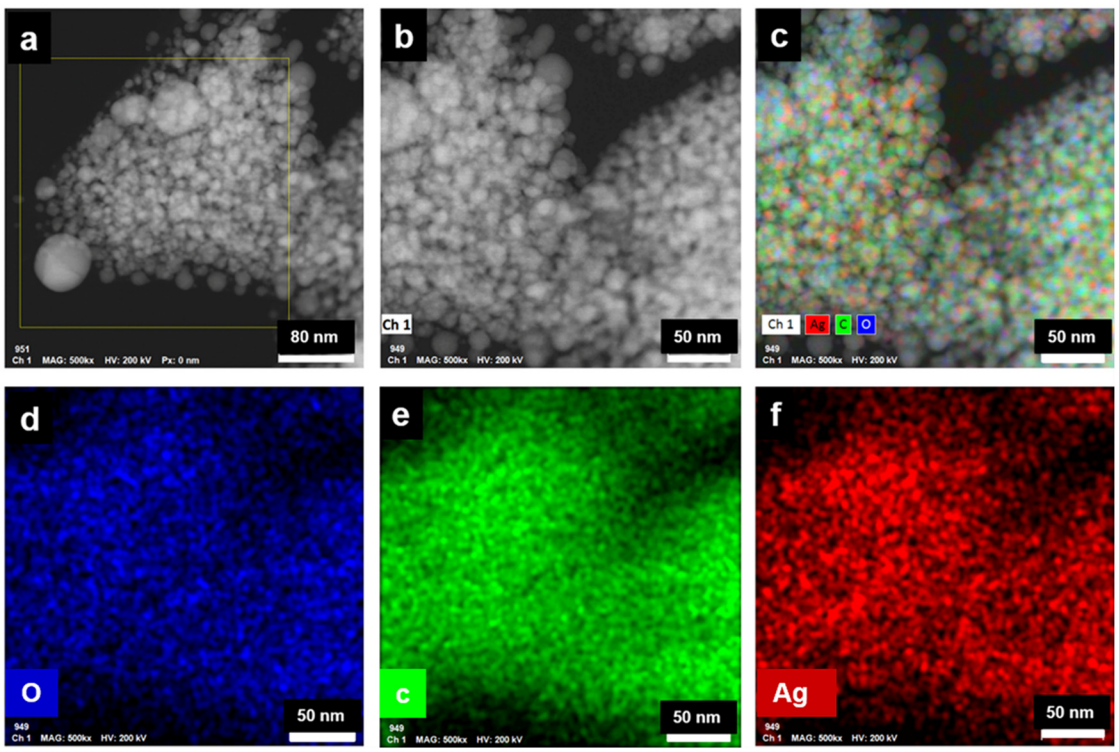

Fig. 3 (a and b) HAADF STEM images of ATP, (c–f) corresponding HAADF STEM elemental mapping images of ATP.

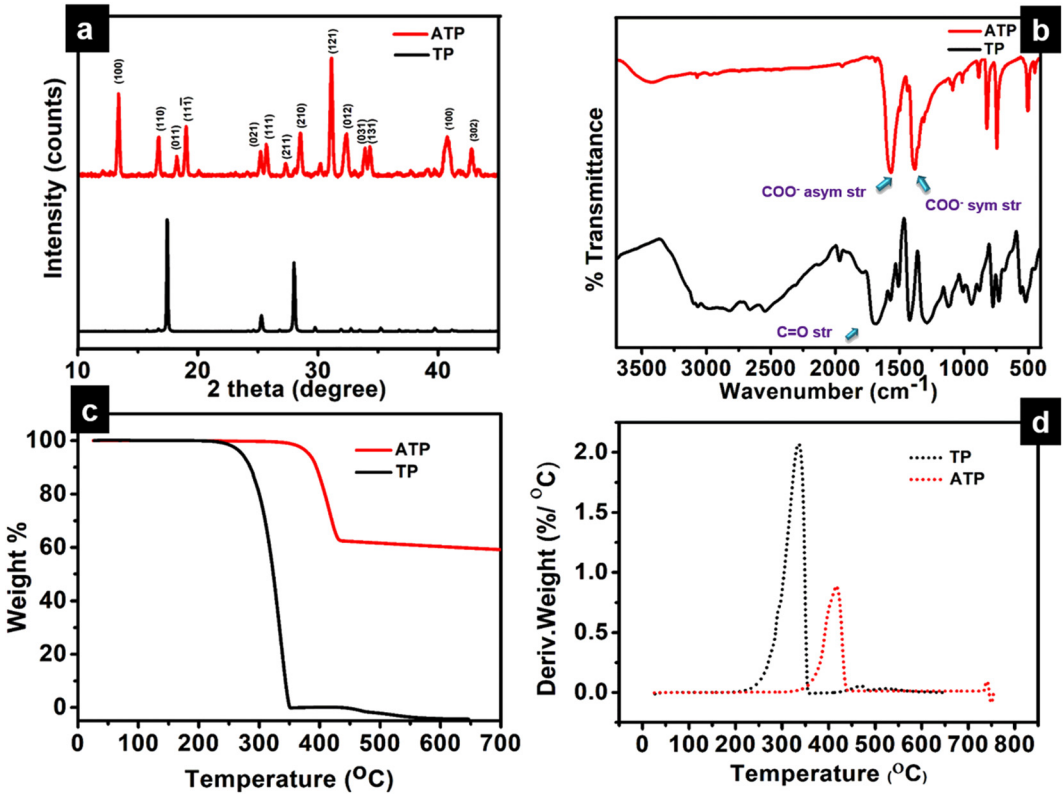

Fig. 4 (a) XRD pattern, (b) FT-IR spectra, (c) TGA curve, and (d) DTG plots of ATP and TP.

atoms belonging to three terephthalate ions and one silver ion through a bridging bond. Bonding between silver and terephthalate ions results in the formation of a three-dimensional framework with an average crystallite size of 32.77 nm, calculated using the Debye–Scherer equation.[21,22] Concomitantly infused silver nanoclusters in ATP did not provide lucid evidences in the XRD spectra owing to their smaller size.

The Ag-OOC bonding in ATP is confirmed from the FT-IR spectrum (Fig. 4b). Peaks at 1564 cm^{-1} and 1378 cm^{-1} correspond to the asymmetric and symmetric stretching vibrations of the carboxylate group of terephthalic acid coordinated to silver, respectively.[21] The C═O stretching frequency of uncoordinated terephthalic acid at 1676 cm^{-1} is not observed in ATP, which confirms the absence of pure terephthalic acid.[23] The nature of the bonding between Ag and the carboxylate group could be qualitatively evaluated by measuring the difference between the symmetric and asymmetric stretching vibrations $\Delta\upsilon$ ($\upsilon_{as} - \upsilon_{s}$) of the COO– group. In the case of ATP, the calculated value is 186 cm^{-1}, which indicates the bridging bidendate bonding between Ag and terephthalate.[24] The broad band centered around 3000 cm^{-1} in the TP spectrum disappears in ATP, indicating the formation of the O–Ag bond.[25] The O–Ag bond is further confirmed from the characteristic weak peak observed at 504 cm^{-1}, while the peak at 740 cm^{-1} corresponds to COO– bending.

Thermal analysis (TGA and DTG) demonstrates the higher thermal stability of ATP, as viewed from Fig. 4c and d. The onset of degradation is at 346 °C, and there is not much weight loss until 346 °C. As the temperature increases to 433 °C, ATP has a weight loss of 37.32%. This indicates that ATP undergoes a ligand-centered decomposition, where fragmentation of the metal–oxygen, oxygen–carbon, and carbon–carbon bonds occur. During the decomposition process, CO_2 and other volatile organic materials are produced, leaving behind silver oxides.[26] The DTG curve of TP designates an onset of degradation at 227 °C with no residual weight at 336 °C. Thermal degradation profiles therefore endorse the excellent thermal stability of ATP when compared to TP, presenting substantial evidences for the existence of strong O–Ag bonds in the MOF network structure of ATP.

Insights into the electronic structure of the elements present in ATP is provided by XPS analysis. The survey spectrum indicates the presence of Ag, C, and O atoms, which are in good agreement with their corresponding binding energies (Fig. 5a). The XPS scan spectra of Ag 3d, C 1s, and O 1s are given in Fig. 5b–d, respectively. The characteristic peaks corresponding to Ag 3d consist of two spin–orbit components – Ag $3d_{5/2}$ and Ag $3d_{3/2}$ at 368.2 eV and 374.2 eV, respectively, with the spin energy separation of 6 eV. The binding energy of an electron in the $3d_{5/2}$ orbital of Ag in ATP is deconvoluted into Ag(1) and Ag(0), and is observed at 369.4 eV and 368.2 eV, respectively.[27] The most intense peak at 284.5 eV of the C 1s spectrum can be attributed to the C atoms of the phenyl ring. The binding energy corresponding to the O–C═O carbon atom of the carboxylate group is obtained at 288.2 eV, while that at

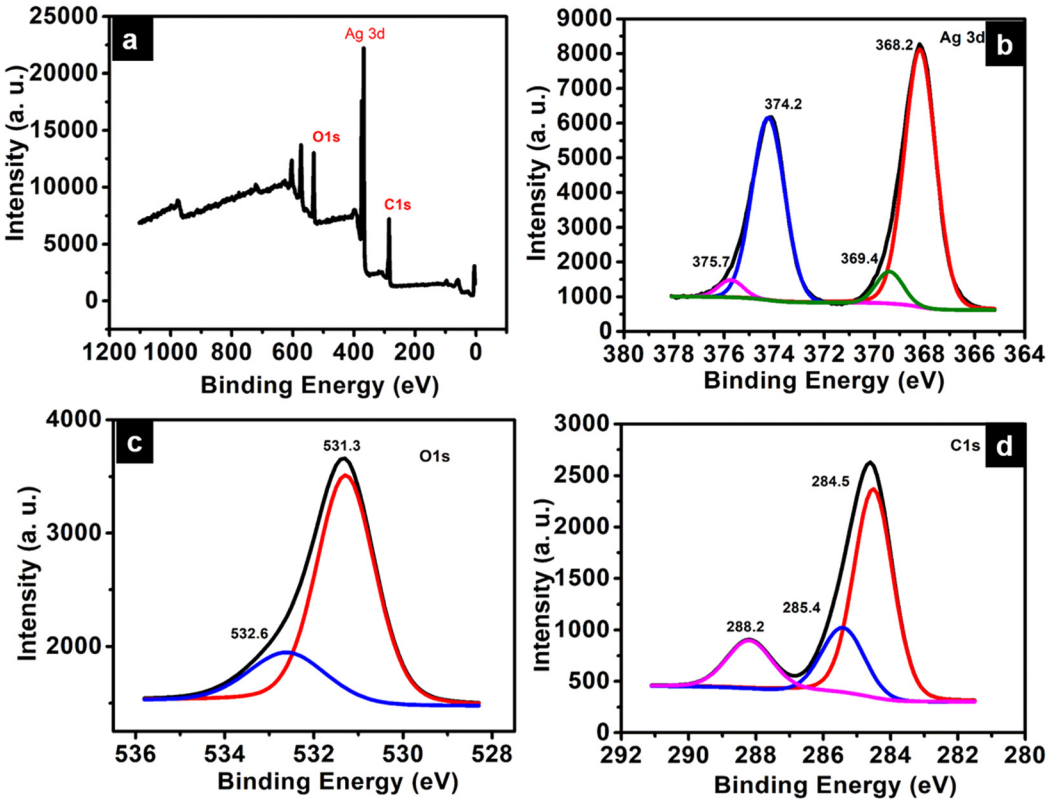

Fig. 5 (a) XPS survey spectrum, (b) high-resolution XPS spectra of Ag 3d, (c) O1s, (d) C1s.

285.4 eV corresponds to the C–O bond.[28] The O 1s peak at 531.3 eV corresponds to C═O of terephthalic acid coordinated to silver. The shoulder peak at 532.6 eV may be due to C–O–H of the unreacted terephthalic acid.[29]

Photoluminescence studies

ATP shows time-resolved long-lived emission. It shows a maximum emission at 520 nm, along with peaks at 485 nm and 557 nm when excited at 340 nm. UV-Vis diffuse reflectance spectra of terephthalic acid and ATP with absorbance maxima at 222 nm (π–π* transition) and 263 nm, respectively, are shown in Fig. 6a and b. Usually, organic luminogens are nonphosphorescent in solution phase due to various intramolecular interactions. However, it has been observed that in the solid state, these luminogens exhibit crystallization-induced emission due to restricted intramolecular interaction, but there exist several intermolecular interactions such as H-bonding.[30]

Pure terephthalic acid (TP) exhibits a steady state photoluminescence with intense blue emission at 386 nm. TP is known to exhibit crystallization-induced dual emissions, such as prompt and delayed fluorescence with two decay lifetimes at 0.53 ns and 0.16 ms due to intermolecular H-bonded interaction between the carboxylate group of terephthalic acid in solid state. It has been observed that the steady state photoluminescence of terephthalic acid coordinated to silver get red-shifted compared to the free ligand. The phosphorescence decay curve of ATP displays a lifetime of 3.91 ms. The strong coordination interaction between the silver ion and terephthalate leads to a rigid conformation, which reduces non-radiative transition and contributes towards ligand-centered phosphorescence. In a structural point of view, TP molecules are confined within the rigid structure of ATP due to the coordination with silver when compared to the two-dimensional structure of pure terephthalic acid with intermolecular interaction.[31] Organic groups containing O and N can enhance the phosphorescence as they could facilitate spin–orbit coupling, thereby effectively reducing the nonradiative decay. The enhanced lifetime of ATP could be further due to the heavy atom effect, which facilitates spin–orbit coupling. Fig. 6d represents the life time decay profile of ATP. Fig. 6e represents the photographic images of ATP and TP in the presence of visible and UV visible light. The Commission International de l'Eclairage (CIE) 1931 chromaticity diagram and colour coordinates of ATP on 340 nm excitation are shown in Fig. 6f. ATP shows green emission with CIE chromaticity coordinates at (0.278, 0.552), which is in accordance with the photographic image of ATP under UV light (365 nm) (Fig. 6e).

Functional applications

Polymer films and thin film coatings. Silver systems are known to exhibit broad spectrum antibacterial activity, while their activity could vary as a function of the size of silver nanoparticles, oxidation state, and other properties. Silver-based nanomaterials of 10 to 100 nm size exhibit significant

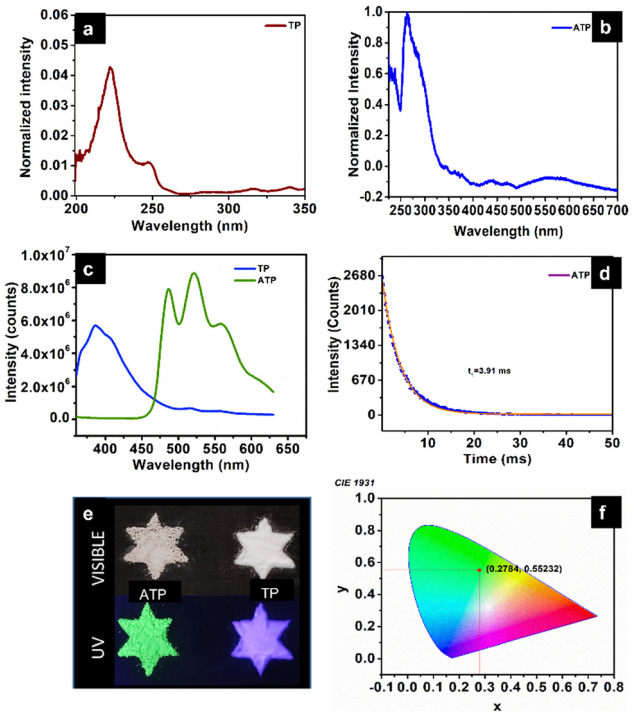

Fig. 6 UV-Vis diffuse reflectance spectra of (a) terephthalic acid and (b) ATP. (c) Steady state photoluminescence spectra of TP and ATP. (d) Lifetime decay profile of ATP. (e) Photographic images of ATP and TP under visible and UV light. (f) CIE 1931 Chromaticity diagram of ATP.

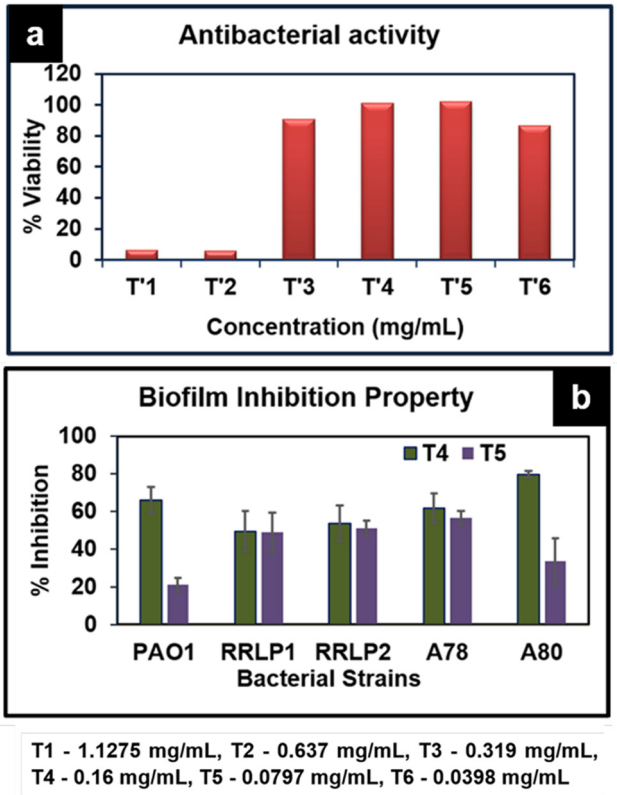

Fig. 7 (a) Antibacterial activity of various concentrations of ATP against *P. aeruginosa* PAO1. (b) Biofilm inhibition of ATP against various bacterial strains PAO1, RRLP1, RRLP2, A78 and A80.

bactericidal activity even against multidrug-resistant bacteria, essentially explained as a function of size, shape, surface charge, oxidation state, and other properties.[32,33]

Among the tested concentrations, the minimum inhibitory concentration (MIC) of ATP against the reference strain *Pseudomonas aeruginosa* PAO1 and clinical isolates *P. aeruginosa* (RRLP1 and RRLP2) was determined as 0.637 mg mL^{-1} for all tested organisms (Fig. 7a), and evaluated by doubling dilution method wherein the concentration was varied from 1.1275 mg mL^{-1} to 0.0398 mg mL^{-1}. In the current investigation, the MIC was taken into consideration as the lowest ATP concentration among the investigated values at which no bacterial growth could be seen. Antibacterial activity of ATP is assigned to its ability to get anchored on the bacterial cell wall surface, which damages the cell functions by penetrating through the membrane and subsequently releases silver ions. Silver ions can form stable bonds with proteins, which play a key role in transmembrane adenosine triphosphate generation.[34] In addition to interaction with proteins, Ag^{+} can intercalate with the base pairs of nucleic acids.[35] Biofilm inhibition study was performed using the sub-MIC doses (0.160 mg mL^{-1} and 0.0797 mg mL^{-1}) of ATP (Fig. 7b).

When bacteria get attached to a surface and subsequently produce an extracellular matrix consisting of polysaccharides and protein, biofilms are generated. The formation of a biofilm is responsible for most of the antibiotic resistance exhibited by several microorganisms.[36] It could be viewed that ATP exhibits significant biofilm inhibition against all tested organisms. Crystal violet staining results indicated that test organisms that are not treated with ATP (control) exhibited an increased absorbance at 570 nm corresponding to elevated biofilm formation. ATP treatment (0.160 mg mL^{-1} and 0.0797 mg mL^{-1}) markedly inhibited biofilm formation compared to the respective control(s). As represented in Fig. 7b, among the tested doses, 0.160 mg mL^{-1} of ATP exhibited significantly higher % reduction in biofilm formation than 0.0797 mg mL^{-1}.

In PAO1, the % biofilm formation was 21.35 ± 3.5 (0.0797 mg mL^{-1}) and 66.0 ± 7.0 (0.160 mg mL^{-1}) Similarly, among the clinical strains of *P. aeruginosa*, 0.16 mg mL^{-1} of ATP exhibited the highest reduction in biofilm formation in the order of 53.81 ± 9.41% and 49.52 ± 10.69% with *P. aeruginosa* RRLP2 and RRLP1, respectively.

Poly(methyl methacrylate) (PMMA), due to its distinct properties, *viz.*, UV transmittance, thermal stability, mechanical properties, chemical resistance and hydrophobic nature, is extensively used for fabrication of nanocomposite films.[37] High quality UV transmittance and low UV absorption properties of PMMA highly favour its use as a nanocomposite film for photoluminescence applications. The FT-IR spectra of the ATP-integrated PMMA films with ATP concentrations varying as 5, 10, 15 wt% along with PMMA (control) are presented in Fig. S1a (ESI†). The intense peak at 1723 cm^{-1} corresponds to –C═O stretching, the carbonyl ester group of PMMA, which is retained in all ATP–PMMA films. The peak observed at

752 cm^{-1} is attributed to C=O bending. The two short bands that appear at 1271 cm^{-1} and 1235 cm^{-1} correspond to the C–O stretching modes of vibrations, while the two small bands appearing at 2845 cm^{-1} and 2999 cm^{-1} could be assigned to the symmetric and asymmetric stretches of CH_3, respectively.[38] The peak at 504 cm^{-1} corresponding to the Ag–O bond is observed in the case of films with higher concentrations of ATP, and is slightly shifted to 524 cm^{-1} due to the interaction between ATP and PMMA. The ATP–PMMA films exhibit two stage degradation unlike ATP, which has a single step degradation, as indicated by TGA (Fig. S1b, ESI†). The onset of degradation is observed at 90 °C for ATP–PMMA with a continuous weight loss until the temperature reaches 200 °C, which might be due to the loss of volatile components or the degradation of unsaturated end groups.[38] The major decomposition of the PMMA film initiates around 260 °C and continues until 420 °C as a result of the main chain scission. All the TGA profiles, irrespective of ATP concentrations, exhibited a similar trend except in the residual weight, which is in accordance with the ATP concentrations. PL studies of the nanocomposite films exhibit luminescence spectra similar to ATP. ATP–PM 12/5, ATP–PM 12/10, and ATP–PM 12/15 films have lifetimes of 3.63 ms, 3.73 ms, and 3.73 ms, respectively (Fig. 8a–d). The lifetime of

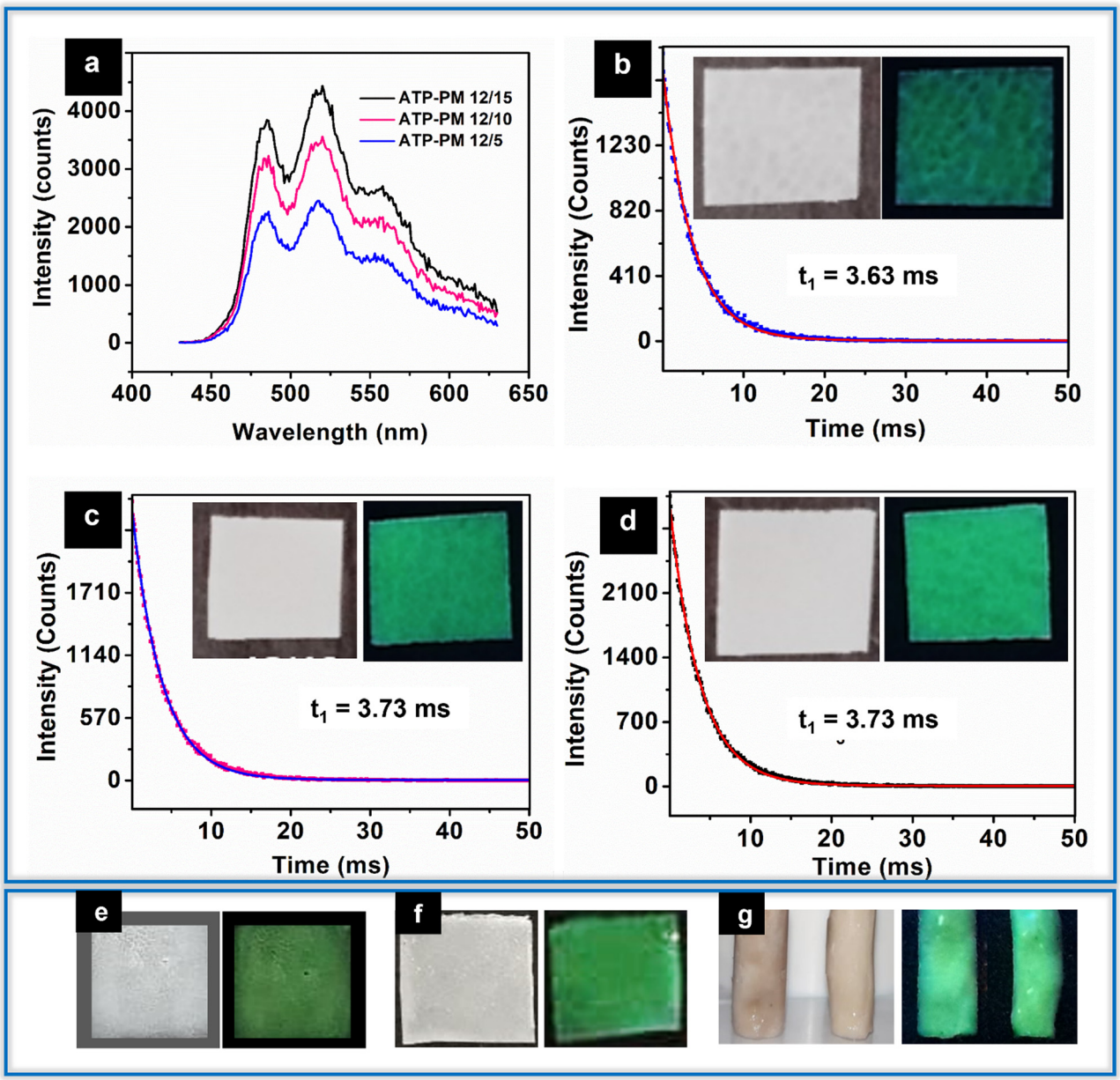

Fig. 8 (a) Photoluminescence spectra of (a) ATP–PM 12/5, ATP–PM 12/10, and ATP–PM 12/15. Life time decay profile of (b) ATP–PM 12/5, (c) ATP–PM 12/10, (d) ATP–PM 12/15 (Inset: photographic image of ATP–PMMA films). Photographic images of (e) ATP/PMMA antibacterial thin film coating under visible light and UV light. (f) ATP/PCL thin film coating under visible light and UV light. (g) ATP/PVA hydrogel under visible and UV light.

ATP is not altered for ATP–PMMA, ensuring its better functionality for optical applications.

Antibacterial and antibiofilm properties of ATP could be further explored as antibacterial coatings. Thin film coatings were made possible by dispersing ATP in PMMA and polycaprolactone (PCL) solution, and subsequently dropping them on glass slides (Fig. 8e and f). A significant modulation in the hydrophobicity of the PCL thin film (contact angle-106.7°) is evident (contact angle-80.7°; hydrophilic) as a result of incorporation of ATP.

Photoluminescent hydrogel. PVA hydrogels are known for its diverse applications due to its high biocompatibility, while the abundance of hydroxyl groups presents a facile opportunity for crosslinking using appropriate chemical reagents. ATP–PVA hydrogels cross-linked with biocompatible crosslinking agent glyoxal (Fig. 8g) exhibited green emission, similar to that of ATP–PMMA films when excited at 365 nm using a UV lamp.

From the results, the underlying mechanism of the long-lived luminescence of ATP could be well correlated to the structure–property relation of the nanocrystals. The heterogeneous nucleation of Ag nanocrystals simultaneously with the MOF formation leads to the evolution of such a distinctive morphology, favouring the distribution of the Ag^0 nanocrystals over and into the ATP MOF. Besides this, the local environment also contributes to the final structure of the compound. Since the Ag^0 nanocrystals are bound on/over ATP, they are relatively passive and stable compared to normal Ag^0 nanocrystals, which undergo faster oxidation. These are the governing factors that contribute to the unique configuration of the supranano clusters, and the PL properties present it as a high-performance multifunctional resource for fabricating optical devices.

Conclusions

The study presents a very photostable long-lived photoluminescent silver terephthalate MOF with a lifetime of 3.91 ms that was synthesized by aqueous one-pot method at room temperature. PL studies and lifetime measurements validated the long lived green luminescent emission, while STEM results complimentary with HRTEM present clear evidences for Ag nanocluster as the key factor for the long-lived luminescence. The as-synthesized ATP is photostable for several months. Diverse advanced functional materials, such as ATP–PMMA films, thin film coatings, hydrogels, were developed using ATP as a smart luminescent resource. The luminescent antibacterial films, coatings and gels pave the ways for the development of more innovative materials using ATP. The results demonstrate ATP as a high functional candidate for a wide variety of novel applications in optical devices, such as LEDs, security systems, and sensors, and as an antibacterial thin film coating.

Author contributions

L. H. G. conceptualized and developed the methodology of the synthesis and investigated the results. S. P. supervised the methodology development. N. M. supervised and carried out PL studies. S. G. S. conceptualized and supervised the entire work, and revised and edited the manuscript. P. R. carried out the antibacterial and biofilm inhibition studies. S. A. contributed to the methodology section. All authors have given approval to the final version of the manuscript.

Conflicts of interest

There are no conflicts to declare.

Acknowledgements

The authors are extremely grateful to Dr. Balagopal Nair, Curtin University, Australia for his efforts in acquiring STEM images, and providing insights into the structure of the silver nanocluster. The authors also acknowledge DST-SAIF Cochin for XRD analysis, NIIST Trivandrum for XPS and IISER Mohali for STEM imaging.

References

1 K. N. Shinde, S. J. Dhoble, H. C. Swart and K. Park, *Phosphate phosphors for solid-state lighting*, Springer Berlin, Heidelberg, 2012.
2 K. V. R. Murthy and H. S. Virk, *Defect Diffus. Forum*, 2014, **347**, 1–34.
3 H. Tan, T. Wang, Y. Shao, C. Yu and L. Hu, *Front. Chem.*, 2019, **7**, 387.
4 J. Liu, L. Yang and F. Luo, *J. Solid State Chem.*, 2021, **301**, 122369.
5 K. Van den Eeckhout, P. F. Smet and D. Poelman, *Materials*, 2010, **3**, 2536–2566.
6 L. Li, W. Wang, J. Tang, Y. Wang, J. Liu, L. Huang, Y. Wang, F. Guo, J. Wang, W. Shen and L. A. Belfiore, *Nanoscale Res. Lett.*, 2019, **14**, 190.
7 M. Pamei and A. Puzari, *Nano-Struct. Nano-Objects*, 2019, **19**, 100364.
8 C. Jiang, Z. Yu, C. Jiao, S. Wang, J. Li, Z. Wang and Y. Cui, *Eur. J. Inorg. Chem.*, 2004, 4669–4674.
9 R.-W. Huang, Y.-S. Wei, X.-Y. Dong, X.-H. Wu, C.-X. Du, S.-Q. Zang and T. C. W. Mak, *Nat. Chem.*, 2017, **9**, 689–697.
10 P.-K. Chow, G. Cheng, G. S. M. Tong, C. Ma, W.-M. Kwok, W.-H. Ang, C. Y.-S. Chung, C. Yang, F. Wang and C.-M. Che, *Chem. Sci.*, 2016, **7**, 6083–6098.
11 W.-P. To, G. S.-M. Tong, W. Lu, C. Ma, J. Liu, A. L.-F. Chow and C.-M. Che, *Angew. Chem., Int. Ed.*, 2012, **51**, 2654–2657.
12 J. H. S. K. Monteiro, *Molecules*, 2020, **25**, 2089.
13 S. Galdiero, A. Falanga, M. Vitiello, M. Cantisani, V. Marra and M. Galdiero, *Molecules*, 2011, **16**, 8894–8918.
14 A. Gibała, P. Żeliszewska, T. Gosiewski, A. Krawczyk, D. Duraczyńska, J. Szaleniec, M. Szaleniec and M. Oćwieja, *Biomolecules*, 2021, **11**, 1–20.
15 C.-R. Wang, K. Kam-Wing Lo and V. W.-W. Yam, *J. Chem. Soc., Dalton Trans.*, 1997, 227–230.

16 X. Jia, J. Li and E. Wang, *Chem. Commun.*, 2014, **50**, 9565–9568.
17 Y. Chen, T. Yang, H. Pan, Y. Yuan, L. Chen, M. Liu, K. Zhang, S. Zhang, P. Wu and J. Xu, *J. Am. Chem. Soc.*, 2014, **136**, 1686–1689.
18 S. Q. Luo, Q. Wang, J. Quan, M. Yang, Y. Wang, X. Zhang and Z. N. Chen, *Transition Met. Chem.*, 2021, **46**, 415–421.
19 G. Didier, C.-G. Eduardo, C. N. Tuan, F. Eduard, B. Wouter, A. Saleh, S. Philomena, D. Francesco, B. Dipanjan, B. J. R. Maarten, N. M. Tho, H. Johan and L. Peter, *Science*, 2018, **361**, 686–690.
20 P. Rathinam, H. S. Vijay Kumar and P. Viswanathan, *Biofouling*, 2017, **33**, 624–639.
21 M. Gutiérrez, C. Martín, B. E. Souza, M. Van Der Auweraer, J. Hofkens and J. Tan, *Appl. Mater. Today*, 2020, **21**, 100817.
22 D. Sun, R. Cao, W. Bi, J. Weng, M. Hong and Y. Liang, *Inorg. Chim. Acta*, 2004, **357**, 991–1001.
23 E. Biemmi, T. Bein and N. Stock, *Solid State Sci.*, 2006, **8**, 363–370.
24 C. M. Crisan, T. Mocan, M. Manolea, L. I. Lasca, F. A. Tăbăran and L. Mocan, *Appl. Sci.*, 2021, **11**, 1–18.
25 J. Liu, Y. Shang, Q. Zhu, X. Zhang and J. Zheng, *Microchim. Acta*, 2019, **186**, 1–8.
26 C. Healy, K. M. Patil, B. H. Wilson, L. Hermanspahn, N. C. Harvey-Reid, B. I. Howard, C. Kleinjan, J. Kolien, F. Payet, S. G. Telfer, P. E. Kruger and T. D. Bennett, *Coord. Chem. Rev.*, 2020, **419**, 213388.
27 Y. Chen, T. Yang, H. Pan, Y. Yuan, L. Chen, M. Liu, K. Zhang, S. Zhang, P. Wu and J. Xu, *J. Am. Chem. Soc.*, 2014, **136**, 1686–1689.
28 Y. Sun, Z. Xue, Q. Liu, Y. Jia, Y. Li, K. Liu, Y. Lin, M. Liu, G. Li and C. Y. Su, *Nat. Commun.*, 2021, **12**, 1–8.
29 E. Desimoni, G. I. Casella, A. Morone and A. M. Salvi, *Surf. Interface Anal.*, 1990, **15**, 627–634.
30 Y. Gong, L. Zhao, Q. Peng, D. Fan, W. Z. Yuan, Y. Zhang and B. Z. Tang, *Chem. Sci.*, 2015, **6**, 4438–4444.
31 X. Yang and D. Yan, *Adv. Opt. Mater.*, 2016, **4**, 897–905.
32 M. K. Rai, S. D. Deshmukh, A. P. Ingle and A. K. Gade, *J. Appl. Microbiol.*, 2012, **112**, 841–852.
33 S. Pal, Y. K. Tak and J. M. Song, *Appl. Environ. Microbiol.*, 2007, **73**, 1712–1720.
34 U. Klueh, V. Wagner, S. Kelly, A. Johnson and J. D. Bryers, *J. Biomed. Mater. Res.*, 2000, **53**, 621–631.
35 Y. Qing, L. Cheng, R. Li, G. Liu, Y. Zhang, X. Tang, J. Wang, H. Liu and Y. Qin, *Int. J. Nanomed.*, 2018, **13**, 3311–3327.
36 B. K. Sharma, A. Saha, L. Rahaman, S. Bhattacharjee and P. Tribedi, *Adv. Microbiol.*, 2015, **05**, 677–685.
37 J. Xu and D. Li, *Polymers*, 2018, **10**, 1217.
38 A. Singhal, K. A. Dubey, Y. K. Bhardwaj, D. Jain, S. Choudhury and A. K. Tyagi, *RSC Adv.*, 2013, **3**, 20913–20921.